Journal of Materials Chemistry B

RSC Publishing

PAPER

View Article Online
View Journal | View Issue

Cite this: J. Mater. Chem. B, 2013, 1, 2289

Crumpled reduced graphene oxide–polyamidoamine dendrimer hybrid nanoparticles for the preparation of an electrochemical biosensor†

Elena Araque,[a] Reynaldo Villalonga,*[a] María Gamella,[a] Paloma Martínez-Ruiz,[b] Julio Reviejo[a] and José M. Pingarrón*[a]

Received 20th January 2013
Accepted 1st March 2013

DOI: 10.1039/c3tb20078g

www.rsc.org/MaterialsB

Reduced graphene nanoparticles were prepared from graphene oxide through a two-step covalent modification approach. Graphene oxide was first enriched with reactive epoxy groups by anchoring (3-glycidyloxypropyl)trimethoxysilane at the hydroxyl groups located on the nanocarbon basal plane. Modified graphene oxide was further cross-linked and partially reduced by treatment with the fourth-generation ethylenediamine core polyamidoamine G-4 dendrimer producing graphene nanoparticles with crumpled paper-like morphology. This graphene derivative was employed as a coating material for glassy carbon electrodes and the nanostructured electrode was tested for the preparation of electrochemical biosensors by immobilizing the enzyme tyrosinase through cross-linking with glutaraldehyde. This bioelectrode showed excellent electroanalytical behavior for catechol with a fast response in about 6 s, linear range of 10 nM to 22 μM, sensitivity of 424 mA M^{-1}, and low detection limit of 6 nM. The enzyme biosensor also showed high stability when stored at 4 °C under dry and wet conditions.

Introduction

Engineering nanomaterials with well-defined three-dimensional morphology has attracted considerable interest in the last few years due to their envisioned applications in the design of novel electronic devices, drug carrier systems and optical and electrochemical sensors. These 3D-shaped nanomaterials can also be employed as building blocks for the construction of original architectures at the nanoscale.[1] In this context, the synthesis of novel hybrid nanomaterials with improved electroconductive properties and capacity to recognize/immobilize analytical biomolecules is a challenge for biosensor technology.[2] In particular, carbon-based nanomaterials have demonstrated their usefulness in designing hybrid nanostructures for successful application in the preparation of biosensors,[3] with recent efforts focused on the use of graphene hybrid derivatives for the construction of electrochemical biosensors[4] due to the relatively low cost, large surface-to-volume ratio and remarkable electrical, mechanical and thermal properties and biocompatibility of this nanomaterial.[5]

However, there are some major obstacles for the application of graphene in the preparation of electrochemical biosensors. Graphene nanosheets are highly hydrophobic, showing very low solubility in water and many organic solvents, and tending to form irreversible agglomerates through strong π–π stacking and van der Waals interactions.[6] Moreover, the absence of chemical functional groups in graphene limits the stable and large immobilization of biomolecules through covalent linkages.[2a] Chemical derivatization of graphene seems to be a rational approach to overcome these disadvantages.[7] However, the possibility of generically tailoring the chemical properties of graphene is limited by its delicate structure, often yielding nanomaterials with poor electroconductive characteristics. For this reason, the development of synthetic strategies for preparing soluble and highly functionalized graphene derivatives with low modification of its basal structure receives considerable attention.

Many synthetic approaches commonly use graphene oxide (GO), a water soluble derivative that can be easily prepared by oxidative treatment of graphite, as the starting material.[8] GO mainly consists of graphene-like sheets,[9] with hydroxyl and epoxide groups on the basal planes and carbonyl and carboxyl groups at the sheet edges.[5] These oxygen functionalities can be selectively used as anchoring points for chemical modification.[8] GO and its derivatives can be easily reduced by chemical, thermal, photothermal, and electrochemical methods, restoring in high yield the structural and electrical conductivity properties of graphene.[2a,8]

[a]Department of Analytical Chemistry, Faculty of Chemistry, Complutense University of Madrid, 28040-Madrid, Spain. E-mail: pingarro@quim.ucm.es; rvillalonga@quim.ucm.es; Fax: +34 913944329; Tel: +34 913944315

[b]Department of Organic Chemistry I, Faculty of Chemistry, Complutense University of Madrid, 28040-Madrid, Spain

† Electronic supplementary information (ESI) available: Characterization of the hybrid nanomaterial, optimization of biosensor construction. See DOI: 10.1039/c3tb20078g

In this work we describe the preparation of a novel polyaminated graphene derivative through the initial modification of GO with (3-glycidyloxypropyl)trimethoxysilane, using the hydroxyl groups at the basal plane as anchoring points. This silanized GO (Sil-GO) was further functionalized and reduced by treatment with the fourth-generation ethylenediamine-core polyamidoamine dendrimer (PAMAM). The resulting hybrid nanomaterial (PAMAM-Sil-rGO) possessed a crumpled paper-like morphology and was employed as a coating material to modify glassy carbon electrodes. The nanostructured electrode was used as a support for the covalent immobilization of enzyme tyrosinase (Tyr, EC 1.14.18.1), in order to evaluate the performance of the resulting Tyr-PAMAM-Sil-rGO electrode as an electrochemical biosensor for catechol.

Materials and methods

Materials

Tyrosinase (5370 U mg^{-1}), (3-glycidyloxypropyl)trimethoxysilane and glutaraldehyde were acquired from Sigma-Aldrich Co. (USA). The ethylenediamine core, PAMAM G-4 dendrimer was purchased from Dendritech, Inc. (USA). Graphene oxide, prepared according to the Hummer's method,[10] was acquired from NanoInnova Technologies (Spain). All other chemicals were of analytical grade.

Apparatus, electrodes and solutions

Cyclic voltammetry and electrochemical impedance spectroscopy experiments were performed using a FRA2 μAutolab Type III potentiostat/galvanostat, and the data were acquired using GPES Ver. 4.9 and Frequency Response Analyser software, respectively (Metrohm Autolab B.V., The Netherlands). Amperometric measurements in stirred solutions at 300 rpm were carried out with a dual-channel ultrasensitive Inbea potentiostat (Inbea Biosensores S.L., Spain). A conventional three-electrode system was employed in all electrochemical studies. The working electrode was a glassy carbon electrode (GCE, 3.0 mm diameter) modified with the PAMAM-grafted graphene derivative and the immobilized enzyme. An Ag/AgCl/KCl (3 M) and a Pt wire were used as the reference and counter electrodes, respectively. The measurements with the biosensor were carried out at 25 °C in 0.1 M sodium phosphate buffer, pH 6.0 (working volume 10 mL). 100 μM catechol solutions in 50 mM sodium phosphate buffer, pH 6.0, were freshly prepared.

The surface morphology of the nanostructured electrodes was investigated by high resolution field emission scanning electron microscopy (FE-SEM) using a JEOL JSM-6335F microscope (JEOL Ltd., Japan). FT-IR spectra were acquired with a Nicolet Nexus 670/870 spectrometer (Thermo Fisher Scientific Inc., USA).

Synthesis of PAMAM-Sil-rGO

Silanized graphene oxide was prepared by dispersion, firstly, of 50 mg GO in 250 mL ethanol by sonication for 1 h. The dispersion was then heated at 65 °C, mixed with 25 mL of a 1% (v/v) ethanolic solution of (3-glycidyloxypropyl)trimethoxysilane and kept under continuous stirring at this temperature for 12 h. The mixture was cooled and filtered and the resulting solid (Sil-GO) was exhaustively washed with ethanol and finally dried in a vacuum. To prepare PAMAM-Sil-rGO, 50 mg Sil-GO were dispersed in 200 mL ethanol by sonication and the dispersion was mixed with 2.5 mL 10% (w/w) ethylenediamine core PAMAM G-4 solution in methanol and stirred at room temperature for 12 h. The mixture was filtered and the solid was washed several times with ethanol and finally dried under a vacuum at room temperature.

Preparation of the enzyme electrode

A bare GCE was first polished to a mirror-like surface with alumina powder (0.3 μM), rinsed thoroughly with double distilled water, successively washed with double distilled water, anhydrous ethanol and acetone in an ultrasonic bath, and dried under N_2 before use. Coating of the polished GCE was accomplished by depositing two 10 μL aliquots of a 0.5 mg mL^{-1} aqueous dispersion of PAMAM-Sil-rGO on the electrode surface and allowing to dry. The modified electrode was then dipped into a 10 mM sodium phosphate buffer solution, pH 5.0, and the potential was cycled between 0.0 and −1.5 V for 20 cycles to obtain a more reduced graphene derivative on the electrode surface.[11]

The enzyme was further immobilized on the modified electrode by dropping 20 μL of 10 mg mL^{-1} tyrosinase solution in 100 mM sodium phosphate buffer, pH 6.0, and then mixing with 4 μL of 25% (v/v) glutaraldehyde. The electrode was kept at 4 °C for 1 h, then washed several times with cold 50 mM sodium phosphate buffer, pH 6.0, and finally stored in a refrigerator until use.

Results and discussion

The different steps involved in the preparation of the hybrid PAMAM-Sil-rGO nanomaterial, as well as the further enzyme immobilization to construct the nanostructured biosensor, are schematically displayed in Fig. 1.

Firstly graphene nanoparticles were prepared through a two-step synthetic approach as shown in Scheme 1. In a first step,

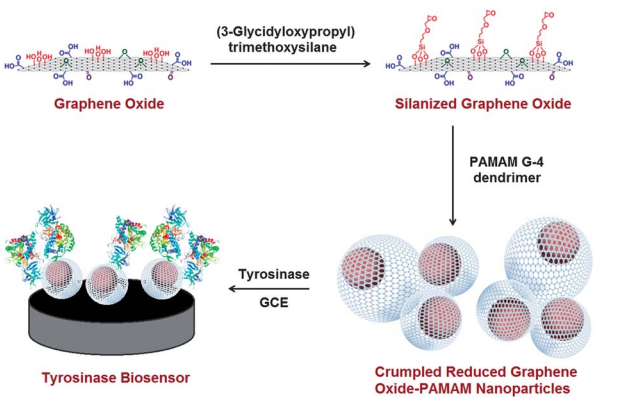

Fig. 1 Schematic display of the steps involved in the preparation of the Tyr/PAMAM-Sil-rGO/GCE enzyme electrode.

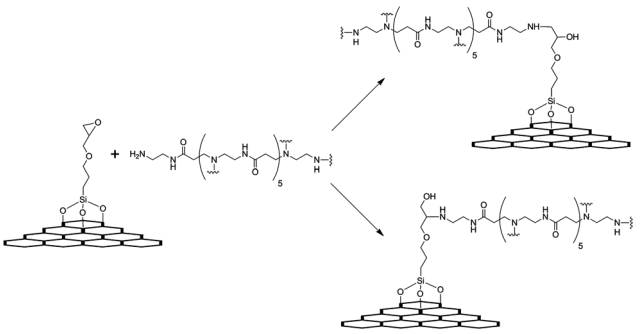

Scheme 1

GO was enriched with reactive epoxy groups by treatment with (3-glycidyloxypropyl)trimethoxysilane, using the hydroxyl groups on the nanomaterial surface as anchoring points.[12] Subsequently, silanized graphene oxide (Sil-GO) was modified with the polyaminated dendrimer molecules through the formation of stable secondary amine linkages according to the reactions shown below, yielding a dark product that was easily dispersed in aqueous solutions (PAMAM-Sil-rGO).

The PAMAM dendrimer was selected as an attractive soft template for GO modification due to its nanosized and monodisperse characteristics exhibiting a regular and highly branched three-dimensional architecture, high structural homogeneity and chain mobility.[13] This soft nanomaterial possesses also a high density of primary amino groups on its surface, which favoured multipoint cross-linking with activated GO sheets.

Characterization of the hybrid nanomaterial

Graphene derivatives were characterized by means of different physico-chemical techniques. Fig. S1 (see ESI†) shows powder XR diffractograms of GO (a), Sil-GO (b) and PAMAM-Sil-rGO (c). The diffractogram of GO shows an intense peak at 12.35° corresponding to a *d*-spacing of about 7.16 Å. This interlayer distance is mainly caused by the presence of oxygen functionalities on GO as well as the water molecules entrapped between the hydrophilic sheets.[14] The intensity of this peak decreased after covalent modification of GO, and it was shifted to 11.50° (7.69 Å) and 10.23° (8.65 Å) after treatment with (3-glycidyloxypropyl)trimethoxysilane and PAMAM, respectively. This increase in the interlayer distance could be ascribed to the bulky silane and dendrimer molecules, which should be intercalated into the interlayer spacing of the nanomaterial. Diffractogram of PAMAM-Sil-rGO also showed a broad and low intensity peak around 20.13° (4.41 Å), which is close to the d_{002}-spacing of graphite (3.35 Å). This small interlayer distance might be attributed to the partial reduction of GO with PAMAM allowing the reduced sheets to pack tighter than the initial nanomaterial.

Fig. S2 (see ESI†) shows the characterization of the graphene derivatives by FT-IR spectroscopy. GO exhibited sharp and broad peaks centered at 3607 cm^{-1} and 3090 cm^{-1} corresponding to the stretching of free and intermolecular H-bonded O–H groups, respectively. In addition, the GO spectrum exhibited the peaks at 1353 cm^{-1} and 1230 cm^{-1} corresponding to the stretching of C–OH and C–O–C groups in unoxidized graphitic domains. The peaks at 1730 cm^{-1} and 1065 cm^{-1} could be ascribed to the stretching of the C=O and C–O groups, respectively. The peak at 1608 cm^{-1} could be associated with the vibrations of unoxidized graphitic skeletal domains, as well as with the adsorbed water.[15]

The presence of silane moieties on the surface of Sil-GO was confirmed by the peaks at 2880 cm^{-1} and 1410 cm^{-1}, which can be ascribed to the stretching and bending of the methylene groups from the (3-glycidyloxypropyl)trimethoxysilane molecules, respectively. Additionally, the peak at 986 cm^{-1} could be associated with the vibration of the Si–O groups. The FT-IR spectrum of PAMAM-Sil-rGO showed that the intensity of the peaks corresponding to the stretching vibrations of the C=O groups at 1730 cm^{-1}, of free O–H groups at 3607 cm^{-1}, of the C–O–C at 1230 cm^{-1} and the C–O at 1065 cm^{-1} decreased significantly, and some of them disappeared totally. This fact suggested that most oxygen functionalities in the Sil-GO sample were reduced during the covalent grafting of PAMAM molecules. The attachment of the dendritic moieties was confirmed by the appearance of the peak at 1541 cm^{-1}, which could be ascribed to the bending of the N–H groups. The broad peak from 2930 to 3506 cm^{-1} could be associated with the stretching vibration of the N–H and O–H groups, as well as with the adsorbed water. However, its multiple peaks pattern also suggested the formation of primary ammonium salts between the attached dendrimer and the remaining carboxylate groups at the graphene sheet edges.

Partial reduction of GO after derivatization with PAMAM was confirmed by electrochemical impedance spectroscopy using $[Fe(CN)_6]^{4-/3-}$ as a redox probe (Fig. 2). Coating of a bare glassy carbon electrode with GO and Sil-GO produced a noticeable increase in the electron transfer resistance (from 256 to 1202 Ω), in agreement with the poor electro-conducting properties of these derivatives. However, the PAMAM-Sil-rGO coated electrode showed a very small semicircle diameter at high frequencies, R_{ct} = 92 Ω, indicating a fast electron transfer process. This observation can be justified by the partial recovery of the characteristic electro-conductive properties of graphene

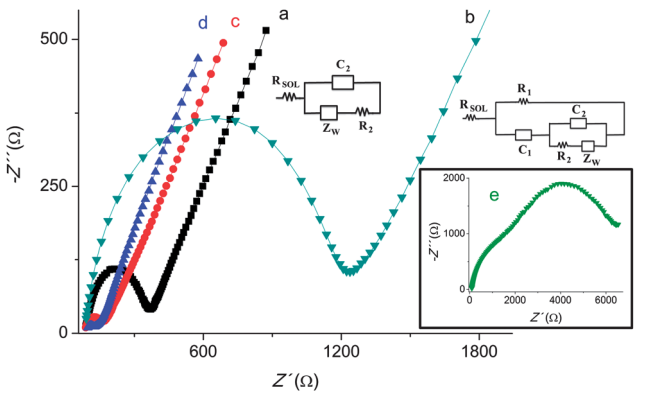

Fig. 2 Impedance plane diagram (−*Z*′′ *versus Z*′) for the EIS measurements at a glassy carbon electrode before (a) and after coating with Sil-GO (b), PAMAM-Sil-rGO (c) PAMAM-Sil-GO after electrochemical reduction (d), and Tyr/PAMAM-Sil-GO (e, inset) in a 0.1 M KCl solution containing 5 mM $K_3[Fe(CN)_6]/K_4[Fe(CN)_6]$ (1 : 1).

after covalent grafting of PAMAM on Sil-GO. The electron transfer resistance decreased even more, $R_{ct} = 24\ \Omega$, upon electrochemical reduction of PAMAM-Sil-rGO on the electrode surface,[11] indicating that grafting of the PAMAM dendrimer on the silanized GO caused only a partial reduction of the nanomaterial, as revealed by FT-IR and XRD analysis. All the experimental data were obtained by fitting with a conventional Randles equivalent circuit.

Modification with (3-glycidyloxypropyl)trimethoxysilane improved thermal stability to GO, as revealed by thermal analysis (see Fig. S3 in the ESI†). However, covalent grafting of PAMAM yielded a derivative exhibiting a thermal-induced transformation at a relatively low temperature, due to decomposition of the dendrimer.

Topological analysis of these nanomaterials was performed by AFM, as shown in Fig. 3. The initial GO sample showed almost exclusively platelets 0.8–1.0 nm thick in agreement with that reported for this material.[16] As expected, silanization of GO increased slightly the average thickness of this flat nanomaterial to about 0.8–1.2 nm due to the presence of covalently bound GPTS moieties above and below the original GO plane. A very different topological pattern was observed for PAMAM-Sil-rGO characterized by the presence of colloidal structures with a variety of sizes and shapes. Crumpled nanoparticles were mainly detected by AFM, but other bulky submicrometer aggregates and some creased sheets were also observed.

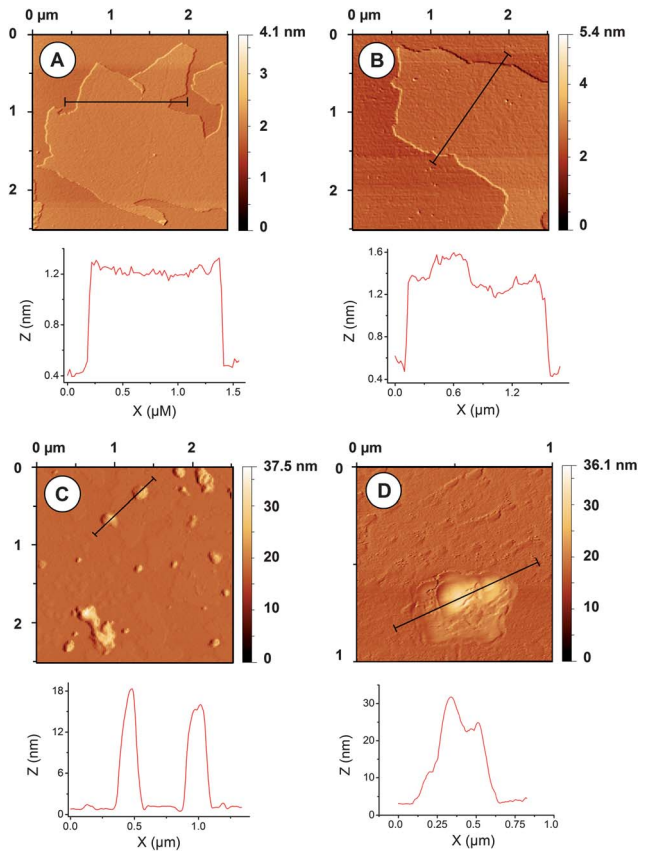

Fig. 3 AFM and section analysis for GO (A), Sil-GO (B) and PAMAM-Sil-rGO (C and D).

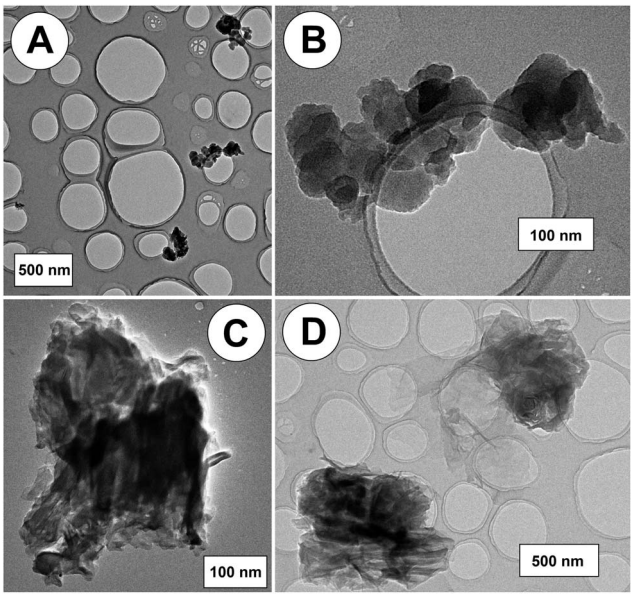

Fig. 4 TEM images of PAMAM-Sil-rGO at low (A) and high (B–D) magnification.

Fig. 4 shows TEM images of the PAMAM-Sil-rGO nanomaterial. It was confirmed that GO sheets were crumpled into three-dimensional nanostructures after covalent modification with the dendrimer. The shape of these nanomaterials varied from compact nanoparticles (Fig. 4A and B) to less ordered structures (Fig. 4C and D), in which pedant and wrinkling graphene sheets were observed in some cases. In addition, some partially creased graphene sheets were also detected. The graphene nanoparticles showed high polydispersity with a diameter distribution ranging from 100 nm to 850 nm, and with a peak size of 420 nm.

Fig. 5 shows HR-TEM images of a crumpled nanostructure. Lattice fringes are visible at the edges of PAMAM-Sil-rGO due to the folding and/or rolling of the sheets. The inter-layer spacing between neighbouring fringes was determined to be 0.472 nm, which is larger than the interplanar spacing in graphite (0.340 nm),[17] but similar to those estimated by XRD, thus confirming the graphene nature of the hybrid material. This fact can be attributed to the presence of silane and dendrimer molecules on the basal plane of the reduced graphene oxide sheets. Using selected area electron diffraction analysis, the

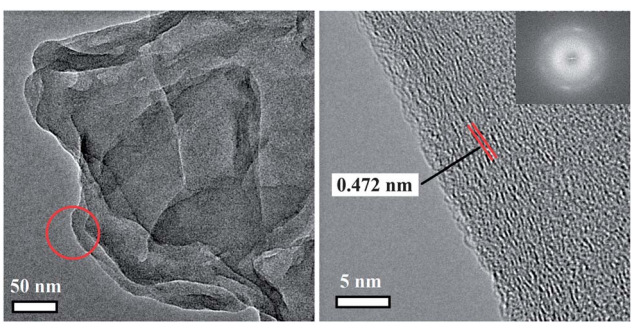

Fig. 5 HR-TEM images of crumpled PAMAM-Sil-rGO.

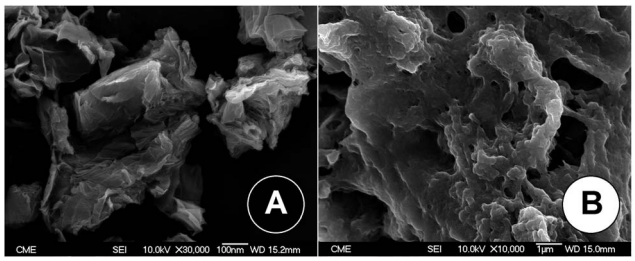

Fig. 6 FE-SEM images of PAMAM-Sil-rGO (A) and Tyr/PAMAM-Sil-rGO (B).

crumpled nanosheets showed a diffuse pattern with six fold symmetry suggesting low crystallinity of the crumpled PAMAM-Sil-rGO derivative.

The morphology of the nanoparticles was also studied by FE-SEM, as illustrated in Fig. 6A. Additional FE-SEM images of these crumpled nanostructures are also provided in Fig. S4 (see ESI†). The crumpled morphology of the PAMAM-Sil-rGO nanoparticles was confirmed, but it was also revealed that they can be formed either by crumpling of a single graphene sheet or by the association of several of these nanomaterials. In some cases, it seems that a single graphene sheet can be involved in the formation of two or more nanoparticles yielding larger and more complex condensed structures. This fact can contribute to the high size polydispersity exhibited by the crumpled nanostructures. It should also be noted that graphene oxide prepared by the Hummer's method[10] is a highly polydisperse material, with sheets ranging from hundred nanometers to several micrometers in size.[18] Thus, the production of crumpled nanostructures with a great variety of diameters can be expected.

It is proposed that the multipoint derivatization of Sil-GO with the polyaminated dendrimer probably induced the crumpling and folding of the carbonaceous sheets around the soft PAMAM templates, yielding three-dimensional nanostructures with an expected polydispersity in sizes showing smaller dimensions than the original unfolded sheet. In addition to this covalent-mediated folding mechanism, the graphene-based nanoparticles could be stabilized by the electrostatic interaction between the carboxylate groups remaining at the platelets edges and the primary amino groups on the dendrimer surface.

It should be highlighted that the random attachment of PAMAM residues on both basal planes of Sil-GO also ensures the location of polyaminated dendrimer moieties on the surface of the folded nanoparticles. This amino-enriched hydrophilic coating provides stability to the graphene nanoparticles in aqueous dispersions as well as the possibility of functionalizing with biomolecules for advanced bioapplications.

Tyrosinase enzyme biosensor at graphene derivative hybrid nanomaterial-modified electrodes

As depicted in Fig. 1, the PAMAM-Sil-rGO hybrid nanomaterial was employed as a modifier of glassy carbon electrodes and, after a further reduction step of the graphene derivative on the electrode surface by cycling the potential between 0.0 and −1.5 V for 20 cycles, the enzyme tyrosinase was covalently immobilized on the nanostructured electrode.

A noticeable smooth and homogeneous morphology was observed for PAMAM-Sil-rGO/GCE after enzyme immobilization (Fig. 6B), without patches of graphene derivatives exposed, suggesting a high protein loading on the electrode surface. Moreover, the EIS spectrum obtained upon immobilization of tyrosinase on PAMAM-Sil-rGO/GCEs caused a noticeable increase in the electron transfer resistance with an overall R_{ct} value of 7837 Ω (Fig. 2, curve e, inset) as a consequence of the significant insulating effect of the protein, indicating also the high enzyme loading on the electrode. In this case, the modified equivalent circuit depicted in the inset of Fig. 2, used for protein-coated electrodes,[19] was employed to fit the experimental data.

The behaviour of the constructed Tyr/PAMAM-Sil-rGO/GCE as an enzyme electrode was checked using catechol as the substrate. Fig. 7 shows cyclic voltammograms recorded before and after addition of catechol at different concentrations. As can be observed, the cathodic current, associated with the electrochemical reduction of the 1,2-benzoquinone formed through the enzyme-catalyzed reaction at the electrode surface, increased with the concentration of catechol added.

The experimental variables involved in the bioelectrode preparation were optimized with regard to the slope of the amperometric response toward concentration ranging from 100 nM to 500 nM (see Fig. S5 in the ESI†). Firstly, the loading of PAMAM-Sil-rGO on the electrode was evaluated. Fig. S5A† shows an increase in the current measured at −150 mV with increasing the amount of hybrid nanomaterial from 2.5 μg to 10 μg. However, the electrode response was lower for loadings larger than 10 μg, which can be attributed to low stability of the nanomaterial layer.

The effect of enzyme loading on the biosensor response is shown in Fig. S5B.† Larger amperometric signals, leading to more suitable calibration curves, were obtained when 200 μg of tyrosinase were used to prepare the biosensor. In addition, the glutaraldehyde concentration used to cross-link the enzyme molecules on the PAMAM-Sil-rGO/GCE surface and the

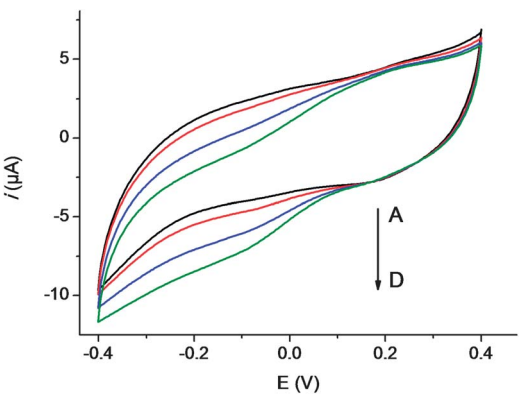

Fig. 7 Cyclic voltammograms recorded at the Tyr/PAMAM-Sil-rGO/GCE in 0.1 M sodium phosphate buffer, pH 6.0, at a scan rate of 50 mV s^{-1} before (A) and after addition of 5 μM (B), 10 μM (C) and 20 μM catechol.

corresponding time of incubation were also optimized. 4% (v/v) glutaraldehyde for 1 h (Fig. S5C and D†) were shown to be the optimum working conditions.

Obviously, operational conditions such as the applied detection potential and the pH value should affect also the biosensor response. The results shown in Fig. S5E and F† revealed that an optimum steady state current was measured when the working potential was fixed at −150 mV. Moreover, a bell-shaped curve was observed for the biosensor amperometric responses as a function of pH, giving the highest current at pH 6.0. Accordingly, these values were selected to carry out further experiments.

The response to catechol of the biosensor configuration prepared with the PAMAM-Sil-rGO-modified electrode was compared with that obtained for other control electrodes (see Fig. S6 in the ESI†). As expected, no response occurred with the nanostructured electrode without enzyme, thus demonstrating that the oxidation of catechol to 1,2-benzoquinone was not electrocatalyzed on the PAMAM-Sil-rGO/GCE surface. In addition, only 30% of the Tyr-PAMAM-Sil-rGO biosensor was obtained with the bioelectrode prepared by immobilizing the enzyme without glutaraldehyde, indicating that covalent cross-linking increased the amount of tyrosinase loaded on the electrode surface. Noticeably lower analytical responses were also achieved when tyrosinase was immobilized, probably by the combined occurrence of enzyme adsorption/cross-linking processes on the electrode surfaces, on bare and Sil-rGO coated GCEs. Therefore, these results supported the proposed design of the Tyr/PAMAM/Sil-rGO/GCE to be used for biosensing purposes.

The enzyme biosensor constructed with this novel graphene-based hybrid nanomaterial showed excellent electroanalytical performance. Fig. 8A shows the amperometric responses of the Tyr/PAMAM-Sil-rGO/GCE biosensor upon continuous addition of catechol. The biosensor exhibited a fast analytical response, producing 95% of the steady-state current within 6 seconds after the addition of catechol.

As illustrated in Fig. 8B, the measured steady state current shows a linear dependence ($r^2 = 0.9974$) with catechol concentration in the 10 nM to 22 μM range ($n = 12$), according to the following equation:

$$i_c\,(\mathrm{mA}) = 424 \times c\,(\text{catechol per M}) - 3.7 \times 10^{-5}$$

This linear range was broader that those reported for tyrosinase biosensors based on the phosphate-doped polypyrrole film on Pt electrode (10 μM–120 μM),[20] *p*-toluene sulfonate-doped polypyrrole film on GCE (5.6 μM–74.3 μM),[21] cyclodextrin-coated magnetic nanoparticles on GCE (100 nM–12 μM),[22] polypyrrole film on Pt electrode (1.0 μM–16 μM),[23] and polyamidoamine dendron-coated gold nanoparticles network on Au electrodes (50 nM–10 μM).[2b] Moreover, the range of linearity of this biosensor was similar, but ranging in a different concentration region, to those reported for tyrosinase biosensors using Fe_3O_4 nanoparticles/chitosan/GCE (83 nM to 70 μM)[24] and polyaniline/ionic liquid/carbon nanofiber/GCE (0.4 nM to 2.1 μM).[25]

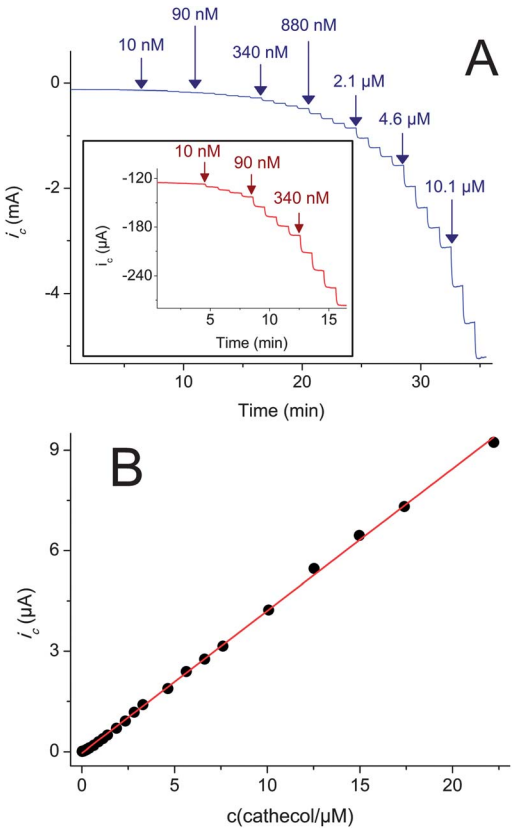

Fig. 8 Amperometric responses (A) and calibration curve (B) obtained with the Tyr/PAMAM-Sil-rGO/GCE for different catechol concentrations. $E_{app} = -150$ mV.

The biosensor constructed showed a very high sensitivity of 424 mA M^{-1}, which was similar to that reported for a tyrosinase biosensor using chitosan/C-coated Ni nanoparticles/GCE (514 mA M^{-1}),[26] but significantly higher than those reported for Tyr/ZnO nanorods/CGE (2.14 mA M^{-1}),[27] Tyr/poly(*N*-3-aminopropyl pyrrole-*co*-pyrrole)/ITO electrode (3.46 mA M^{-1}),[28] Tyr/phosphate-doped polypyrrole/Pt (47 mA M^{-1}),[20] Tyr/PAMAM-Au nanoparticles/Au (19 mA M^{-1}),[2b] and Tyr/3-mercaptopropionic acid/Au (34.2 mA M^{-1})[29] biosensors.

The limit of detection achieved, 6 nM, was calculated according to the $3S_b/m$ criterion, where m is the slope of the calibration curve and S_b was estimated as the standard deviation of 10 different amperometric signals recorded for the lowest catechol concentration measured in the calibration graph (10 nM). This value was lower than those reported for the biosensors constructed with Tyr/3-mercaptopropionic acid/Au (110 nM),[29] Tyr/PAMAM-Au nanoparticles/Au (20 nM),[2b] Tyr/Fe_3O_4 nanoparticles/chitosan/GCE (25 nM),[24] Tyr/ZnO nanorods/CGE (4 μM),[27] Tyr/phosphate-doped polypyrrole/Pt (840 nM),[20] Tyr/*p*-toluene sulfonate-doped polypyrrole/GCE (1.5 μM),[21] and Tyr/polypyrrole/Pt (1.0 μM).[23]

The apparent kinetics constants for the catalytic transformation of catechol to 1,2-benzohydroquinone on the nanostructured electrode surface were determined by means of the Lineweaver–Burk plots. The calculated values were 37.1 μM and 12.8 μA for K_M and I_{MAX}, respectively. The apparent K_M value was

Table 1 Analytical performance of the Tyr/PAMAM-Sil-rGO/GCE biosensor for different phenolic compounds

Compound	Linear range (μM)	Sensitivity (mA M^{-1})	r^2	LOD[a] (nM)
3,4-Xylenol	0.05–0.6	24.4	0.9980	50
p-Cresol	0.01–0.14	337	0.9874	10
m-Cresol	0.25–1.0	47.2	0.9880	250
Phenol	0.1–0.5	54.1	0.9940	100
Hydroquinone	2.5–58.8	1.0	0.9769	2500
4-Cloro-1-naphthol	—	—	—	—
Catechol	0.01–22	424	0.9974	6

[a] LOD: limit of detection.

about ten-fold lower than that reported for the free enzyme (240 μM),[30] suggesting a favourable microenvironment for the enzyme after immobilization on the PAMAM-Sil-rGO hybrid nanomaterial.

Furthermore, the repeatability of the biosensor toward successive additions of catechol in the range of 100 nM to 3.3 μM was examined, and the R.S.D. of the resulting slopes was 6.8% ($n = 10$). In addition, the electrode-to-electrode repeatability was evaluated by measuring the slope values of the calibration plots constructed with ten biosensors prepared in the same manner. The R.S.D. value was 9.4%, indicating an acceptable repeatability in the biosensor preparation procedure.

Also, the Tyr/PAMAM-Sil-rGO/GCE biosensor was successfully employed to quantify other phenolic compounds able to behave as substrates for tyrosinase. The analytical characteristics of the corresponding calibration curves are reported in Table 1, where it can be observed that an excellent sensitivity was also achieved for other compounds such as *p*-cresol as expected for phenolic compounds with at least one *o*-position free.[29,31]

Finally, the storage stability of the biosensor was tested at 4 °C under dry and wet conditions (50 mM sodium phosphate buffer, pH 7.0). The amperometric responses of the electrodes toward 2.0 μM catechol were then measured over 1 month. The results are displayed in Fig. S7 (see ESI†). The enzyme electrodes exhibited excellent storage stability under both storing conditions, retained full catalytic activity after 25 days at 4 °C. It was noticed that the biosensors retained about 96% and 78% of the initial activity after 1 month of dry and wet storing, respectively. This excellent behaviour suggested that the covalent immobilization of tyrosinase on the polyaminated graphene derivative yielded a highly stable immobilized enzyme adduct, which is strongly retained on the electrode surface without noticeable loss of the active conformation under the storage conditions and time tested.

Conclusions

A novel electroconductive polyaminated hybrid nanomaterial was prepared by grafting PAMAM G-4 dendrimer on silanized graphene oxide. This reduced graphene derivative demonstrated its usefulness as an electrode modifier on which enzymes, in this case tyrosinase, can be immobilized giving rise to bioelectrodes exhibiting excellent analytical performance in terms of high sensitivity and stability. These results suggest that this novel approach offers new possibilities for the use of hydrophilic three-dimensional graphene-based structures in the design of functionalized hybrid nanomaterials suitable to be employed in biosensing applications.

Acknowledgements

R. Villalonga acknowledges Ramón & Cajal contract from the Spanish Ministry of Science and Innovation. Financial support from the Spanish Ministerio de Ciencia e Innovación CTQ2011-24355, CTQ2012-34238 and Comunidad de Madrid S2009/PPQ-1642, Programme AVANSENS is gratefully acknowledged.

Notes and references

1 (*a*) M. B. Cortie and A. M. McDonagh, *Chem. Rev.*, 2011, **111**, 3713; (*b*) J. Hu, T. W. Odom and C. M. Lieber, *Acc. Chem. Res.*, 1999, **32**, 435; (*c*) R. G. Chaudhuri and S. Paria, *Chem. Rev.*, 2012, **112**, 2373; (*d*) S. S. Kinge, M. Crego-Calama and D. N. Reinhoudt, *Langmuir*, 2007, **23**, 8772.

2 (*a*) Y. Liu, X. Dong and P. Chen, *Chem. Soc. Rev.*, 2012, **41**, 2283; (*b*) R. Villalonga, P. Díez, S. Casado, M. Eguílaz, P. Yáñez-Sedeño and J. M. Pingarrón, *Analyst*, 2012, **137**, 342.

3 (*a*) R. Cui, C. Liu, J. Shen, D. Gao, J. J. Zhu and H. Y. Chen, *Adv. Funct. Mater.*, 2008, **18**, 2197; (*b*) J. C. Claussen, M. S. Artiles, E. S. McLamore, S. Mohanty, J. Shi, J. L. Rickus, T. S. Fisher and D. M. Porterfield, *J. Mater. Chem.*, 2011, **21**, 11224; (*c*) R. Villalonga, M. L. Villalonga, P. Díez and J. M. Pingarrón, *J. Mater. Chem.*, 2011, **21**, 12858; (*d*) B. Su, D. Tang, J. Tang, Q. Li and G. Chen, *Anal. Biochem.*, 2011, **417**, 89; (*e*) K. Scida, P. W. Stege, G. Haby, G. A. Messina and C. D. García, *Anal. Chim. Acta*, 2011, **691**, 6.

4 (*a*) B. G. Choi, H. S. Park, T. J. Park, M. H. Yang, J. S. Kim, S. Y. Jang, N. S. Heo, S. Y. Lee, J. Kong and W. H. Hong, *ACS Nano*, 2010, **4**, 2910; (*b*) F. Xiao, Y. Li, X. Zan, K. Liao, R. Xu and H. Duan, *Adv. Funct. Mater.*, 2012, **22**, 2487; (*c*) Y. Shao, J. Wang, H. Wu, J. Liu, I. A. Aksay and Y. Lin, *Electroanalysis*, 2010, **22**, 1027.

5 M. J. Allen, V. C. Tung and R. B. Kaner, *Chem. Rev.*, 2010, **110**, 132.

6 X. Yang, J. Zhu, L. Qiu and D. Li, *Adv. Mater.*, 2011, **23**, 2833.

7 (*a*) Y. Si and E. T. Samulski, *Nano Lett.*, 2008, **8**, 1679; (*b*) F. M. Koehler, A. Jacobsen, K. Ensslin, C. Stampfer and W. J. Stark, *Adv. Mater.*, 2011, **23**, 2833.

8 D. R. Dreyer, S. Park, C. W. Bielawski and R. S. Ruoff, *Chem. Soc. Rev.*, 2010, **39**, 228.

9 J. P. Rourke, P. A. Pandey, J. J. Moore, M. Bates, I. A. Kinloch, R. J. Young and N. R. Wilson, *Angew. Chem., Int. Ed.*, 2011, **50**, 3173.

10 W. S. Hummers and R. E. Offeman, *J. Am. Chem. Soc.*, 1958, **80**, 1339.

11 B. Jiang, M. Wang, Y. Chen, J. Xie and Y. Xiang, *Biosens. Bioelectron.*, 2012, **32**, 305.

12 B. Scheibe, E. Borowiak-Palen and R. J. Kalenczuk, *J. Alloys Compd.*, 2010, **500**, 117.
13 F. Vögtle, G. Richardt and N. Werner, *Dendrimer chemistry: concepts, synthesis, properties, applications*, Wiley-VCH, Weinheim, 2009.
14 S. Park, J. An, I. Jung, R. D. Piner, S. J. An, X. Li, A. Velamakanni and R. S. Ruoff, *Nano Lett.*, 2009, **9**, 1593.
15 J. F. Shen, Y. Z. Hu, M. Shi, X. Lu, C. Qin, C. Li and M. G. Ye, *Chem. Mater.*, 2009, **21**, 3514.
16 S. Stankovich, R. D. Piner, X. Chen, N. Wu, S. T. Nguyen and R. S. Ruoff, *J. Mater. Chem.*, 2005, **16**, 155.
17 G. Lu, S. Mao, S. Park, R. S. Ruoff and J. Chen, *Nano Res.*, 2009, **2**, 192.
18 J. E. Kim, T. H. Han, S. H. Lee, J. Y. Kim, C. W. Ahn, J. M. Yun and S. O. Kim, *Angew. Chem., Int. Ed.*, 2011, **50**, 3043.
19 D. Tang, R. Yuan and Y. Chai, *J. Phys. Chem. B*, 2006, **110**, 11640; C. C. Wu, C. H. Lin and W. S. Wang, *Talanta*, 2009, **79**, 62.
20 C. Apetrei, M. L. Rodríguez-Méndez and J. A. De Saja, *Electrochim. Acta*, 2011, **56**, 8919.
21 A. Rajesh, W. Takashima and K. Kaneto, *React. Funct. Polym.*, 2004, **59**, 163.
22 P. Díez, R. Villalonga, M. L. Villalonga and J. M. Pingarrón, *J. Colloid Interface Sci.*, 2012, **386**, 181.
23 Q. Ameer and S. B. Adeloju, *Sens. Actuators, B*, 2009, **140**, 5.
24 S. Wang, Y. Tan, D. Zhao and G. Liu, *Biosens. Bioelectron.*, 2008, **23**, 1781.
25 J. Zhang, J. Lei, Y. Liu, J. Zhao and H. Ju, *Biosens. Bioelectron.*, 2009, **24**, 1858.
26 L. Yang, H. Xiong, X. Zhang and S. Wang, *Bioelectrochemistry*, 2012, **84**, 44.
27 L. Chen, B. Gu, G. Zhu, Y. Wu, S. Liu and C. Xu, *J. Electroanal. Chem.*, 2008, **617**, 7.
28 A. Rajesh, W. Takashima and K. Kaneto, *Sens. Actuators, B*, 2004, **102**, 271.
29 S. Campuzano, B. Serra, M. Pedrero, F. J. M. Villena and J. M. Pingarrón, *Anal. Chim. Acta*, 2003, **494**, 187.
30 J. L. Smith and R. C. Krueger, *J. Biol. Chem.*, 1962, **237**, 1121.
31 J. C. Espín, P. A. García-Ruiz, J. Tudela and F. García-Cánovas, *Biochem. J.*, 1998, **331**, 547.

